J Mater Sci (2008) 43:3101–3111
DOI 10.1007/s10853-008-2521-5

Microstructural changes induced in Portland cement-based materials due to natural and supercritical carbonation

Ana Hidalgo · Concha Domingo · Carlos Garcia · Sabine Petit · Carmen Andrade · Cruz Alonso

Received: 19 September 2007 / Accepted: 31 January 2008 / Published online: 28 February 2008

Abstract Supercritical carbonation of Portland cement binders was studied to analyse the influence of the type of cement on carbonation at high CO_2 pressures (CO_2 at 20 MPa and 318 K) and to improve the understanding of the effects on the microstructure and physicochemical properties of binders. The results were compared with those obtained in a natural exposure. Microstructural properties of supercritically and atmospherically carbonated Portland cement binders were examined using the complementary analytical techniques of FTIR, TG-DTA, and BSEM-EDX. Supercritically carbonated binders showed a microstructure based on a more polymerized and lower Ca form of CSH gel, formed by decalcification of high-Ca form of CSH gel. Results suggested that during the treatment at artificially intensified conditions, the crystallized calcium carbonate came mainly from the carbonation of the CSH gel, and at atmospheric conditions, from the carbonation of the portlandite phase.

A. Hidalgo (✉) · C. Andrade · C. Alonso
Instituto de Ciencias de la Construcción "Eduardo Torroja", CSIC, Serrano Galvache, 4, Madrid 28033, Spain
e-mail: ahidalgo@ietcc.csic.es

C. Domingo · C. Garcia
Instituto de Ciencia de Materiales de Barcelona, CSIC, Campus UAB, Bellaterra 08193, Spain

S. Petit
CNRS UMR 6532 HydrASA, Université de Poitiers, 40, avenue du Recteur Pineau, Poitiers Cedex 86022, France

Introduction

The microstructure of the hardened paste after it has totally or partially reacted with supercritical CO_2 has been relatively little explored, although it is of considerable practical interest, since it affects the properties of carbonated cement, such as strength, capillarity, permeability, and gas diffusivity [1, 2].

Accelerated carbonation is still a developing technology, but the process is commercially potentially valuable for the production of a broad range of desirable carbonated cement-based materials. In fact, carbonation of concrete has demonstrated to act positively in the immobilization of hazardous wastes contaminated with heavy metals and other inorganic pollutants, or even radioactive compounds [3–7]. Carbonation is also attracting an increased interest for the treatment of contaminated soils and the sequestration of CO_2 [8].

Used methods for cement carbonation involve the natural and the accelerated processes [9–11]. In the first case, samples are stored in contact with atmosphere. In artificially intensified carbonation, samples are exposed to pure CO_2. Although the advantages of treating hardened cement pastes with high-pressure CO_2 and $SCCO_2$ have been demonstrated, literature concerned with carbonation at elevated pressures and temperatures is less common [1, 6, 7, 12–14].

Most of the work carried out on the carbonation of cementitious materials has been concentrated on the variations of the microstructure and, hence, on the mechanical properties, of these materials in contact with CO_2 as a function of the type of cement used to produce the concrete. Different authors [15–19] have investigated the effects of carbonation on pore structure, changes of specific surface area using BET theory, permeability, and

diffusional properties of hydrated cement pastes and mortars. Recently García-González et al. and Fernández Bertos et al. [8, 18, 19] discussed the variations of different properties (permeability, porosity, tortuosity, and pore size distribution) as a consequence of the carbonation process in cement-based materials. Additionally a few comparative studies on carbonation have been carried out on cement samples, resulting that the microstructure of cement pastes carbonated using $SCCO_2$ was different than that of air-carbonated pastes. Supercritical carbonation of cementitious materials increases strength and reduces permeability, which are desirable properties for matrices used to immobilize radioactive wastes [8, 18–20].

The purpose of this paper is to provide further evidence and improved understanding of the effects of supercritical carbonation on the microstructure and physicochemical properties of cement pastes, and to analyse the influence of the type of cement on carbonation at high CO_2 pressures. The changes of the microstructure were followed by mid-infrared spectroscopy (FTIR), thermal analysis (DTA/TGA), and backscattering electron microscopy with chemical analysis (BSEM/EDX). A comparison with results obtained in a natural exposure is also made. The sensitivity of infrared spectroscopy to components of a complex mixture is often very different from that of other techniques. Carbonate groups can be recognized by infrared spectroscopy while their presence can be uncertain from X-ray diffraction. DTA/TGA in conjunction with FTIR is able to differentiate between phases with different Ca/Si ratios, besides analysing crystalline or amorphous phases. Backscattering electron microscopy with microanalysis allows to make a mapping of samples and to obtain the variation of Ca/Si ratio and to identify the introduction of Al in CSH gel paste.

Experimental procedure

Materials

Two ordinary Portland cements of varying alkalis and Al_2O_3 contents (CEM I and CEM I-SR according to EN 197-1:2000) from Cia. Valenciana de Cementos Portland S.A, Alcalá de Guadaira, Spain, were used for the testing programme. A Class F fly ash according to ASTM C618 (FA with a mean particle size of 18 μm), from Cia. Valenciana de Cementos Portland, S.A (Alcalá de Guadaira, Spain), and silica fume (SF with a mean particle size of 26 μm) from Ferroatlántica S.L (A Coruña, Spain) were included in binders in a cement replacement basis. Formulations of binders are presented in Table 1; pastes were fabricated with a 0.4 water-to-cement ratio and hydrated for 7 days in sealed conditions (98% relative humidity and 20 ± 1 °C).

Table 1 Formulations of binders

Sample	Formulation
C-1	100% CEM I-SR
C-2	56%CEMI-SR
	35% FA
	9% SF
C-3	100% CEM I

The cement pastes used in this study were mainly granulated powder, although some monolithic pieces ($\sim$0.2 cm^3) were also processed using the supercritical method.

Chemical composition of mineral additions and cements used in this work is shown in Table 2. Na_2O, K_2O, Fe_2O_3, MgO, and Al_2O_3 were analysed by atomic absorption spectrometry (AAS; model 1100B, Perkin Elmer Corp., Norwalk, CT). CaO and SiO_2 were analysed by a photometric method using EGTA and ammonium molybdate as complexants, respectively. SO_3 was analysed by turbidimetry.

Carbonation methods

High-pressure carbonation experiments were carried out in a high-pressure apparatus with continuous CO_2 flow. Liquified CO_2 was compressed to 20 MPa by means of a membrane pump (Lewa EK-M-210). Cement paste samples (powdered and monoliths) were introduced in a 10-mL tubular reactor placed in an air oven heated to 45 °C. The system pressure was controlled with a back pressure regulator (Tescom 26-1761). After system stabilization, the experimental conditions were maintained at a relatively low flow rate of $SCCO_2$ ($\sim$1–2 L min^{-1}) for 2 h. Samples were labelled SCC.

For natural carbonation, powdered cement pastes were stored for a period of 200 days exposed to laboratory atmosphere at $\sim$20 °C and 40–50% RH (0.03% CO_2). Samples were labelled NC.

Characterization

Mid-infrared spectra of mineral additives and cement pastes were obtained using a Nicolet Magna 510 Fourier transform IR spectrometer (FTIR) equipped with a DTGS detector and a CsI beam splitter. For each sample, 256 scans were recorded in the 4000–250 cm^{-1} spectral range with a resolution of 4 cm^{-1}. The spectra of all the samples were measured using the 12-mm-diameter undried KBr pellets (1.5 mg of sample and 150 mg of KBr).

DTA/TGA data have been obtained from a DTA/TG SEIKO 320U thermal analyser with a resolution of

Table 2 Chemical composition of cements and mineral additions

Chemical analysis (%)	SiO_2	Al_2O_3	Fe_2O_3	CaO (total)	MgO	SO_3	Na_2O	K_2O	CaO (free)
CEM I-SR	18.00	4.85	5.26	62.36	1.84	3.28	0.18	0.35	1.92
CEM I	19.15	5.97	3.65	63.32	2.23	3.45	0.51	0.85	1.61
Fly ash	55.63	27.92	5.51	4.63	2.3	–	0.63	3.25	0.15
Silica fume	91.8	0.59	3.74	1.3	0.92	–	0.15	0.37	0.01

0.01 mg. The sample was taken in a platinum crucible and heated from room temperature to 1,200 °C at a heating rate of 10 °C/min using nitrogen as a medium under static condition. Alumina powder was used as the reference material.

Samples were examined through scanning electron microscopy and microanalysis, using backscattered electron imaging of polished surfaces. Samples were embedded into an epoxy resin, cut, polished, and then coated with carbon. A JEOL JSM 5400 scanning electron microscope (SEM) equipped with a solid-state backscattered detector and a LINK-ISIS energy dispersive (EDX) was used.

Figure 7a highlights the cement–FA interfase after supercritical carbonation. The EDX analysis of areas 1 and 2 indicates that fly ash is partially reacted, and it has formed a CASH matrix as can be observed in spectrum 7a-2.

Results and discussion

FTIR

X-ray diffraction analysis of the fly ash (not shown) indicated that it was mainly composed of mullite, quartz, magnetite, CaO, calcite, and glassy phases. Figure 1a shows the FTIR spectrum of fly ash. The band appearing between 560 and 550 cm^{-1} is associated with the octahedral aluminium present in mullite. The band associated with symmetric stretching vibrations of Si–O–Si (from quartz) and Al–O–Si bonds (tetrahedral aluminium of mullite) appears, however, at 800 cm^{-1}. The band centred at around 1,085 cm^{-1} is assigned to Si–O stretching vibrations of the SiO_4 tetrahedral units. Band appearing at 460 cm^{-1} is associated with O–Si–O bond bending vibrations.

X-ray diffraction analysis of the silica fume indicated that it was amorphous. Figure 1b presents the FTIR spectrum of silica fume. The band at 1,120 cm^{-1} corresponds to asymmetric stretching vibrations of Si–O–Si bridging sequences, the one at 800 cm^{-1} corresponds to symmetric stretching vibrations of Si–O–Si bonds, and the last one at 480 cm^{-1} is associated with O–Si–O bond bending vibration.

Figures 2–4 show the mid-IR spectra for raw and carbonated Portland cement pastes: (a) OH-stretching region, and (b) 2,500–250 cm^{-1} region.

OH environment

Interpretation of the OH-stretching region in the mid-IR spectra ($\sim$2,800–4,000 cm^{-1}) is difficult because bands are broad (see Figs. 2a–4a).

The broad band centred at 3450 cm^{-1} is due to stretching vibrations of O–H groups in H_2O or hydroxyls with a wide range of hydrogen bond strengths. The noticeable intensity decrease of this band for supercritically carbonated pastes is related with the release of water during the carbonation process and its removal.

The band at 3640 cm^{-1} is due to Ca–OH vibrations from portlandite. Intensity of this band is related with the content of portlandite. This band was still evident in most of the samples analysed after the different carbonation treatments, indicating that complete carbonation did not take place. Only the sample C-3 processed under supercritical conditions was fully carbonated (Fig. 4a).

2,000–250 cm^{-1} region

The observed features in Figs. 2b–4b provide useful information about microstructural changes in Portland cement pastes: decalcification of CSH and silicate polymerization, presence of TO_4 condensed tetrahedra in gel chains with T = Si or Al (Si–O–Si or Al–O–Si bonds), identification of calcium carbonate polymorphs, and adsorbed water content.

In hydrated Portland cements, the main mid-IR bands for CSH gels appear at $\sim$970 cm^{-1} (Si–O stretching vibrations of Q^2 tetrahedra, corresponding to Si–OH bonds) and 450–500 cm^{-1} [21] (O–Si–O bending vibration, which is influenced by O–Si–O angle and occupancy of neighbouring sites or polymerization). These mid-IR bands change systematically in frequency and/or intensity with Ca/Si ratio in CSH, which is also related with silicate polymerization.

The strongest absorption band of silicates at 970 cm^{-1}, which is present in raw and naturally carbonated samples, shifts to higher wave numbers in the supercritically carbonated mixtures, which can be attributed to CSH chain polymerization (which is accompanied by a decrease in Ca/Si ratio). Carbonation processes result in splitting of the band at 970 cm^{-1} into a few maxima; this fact agrees with

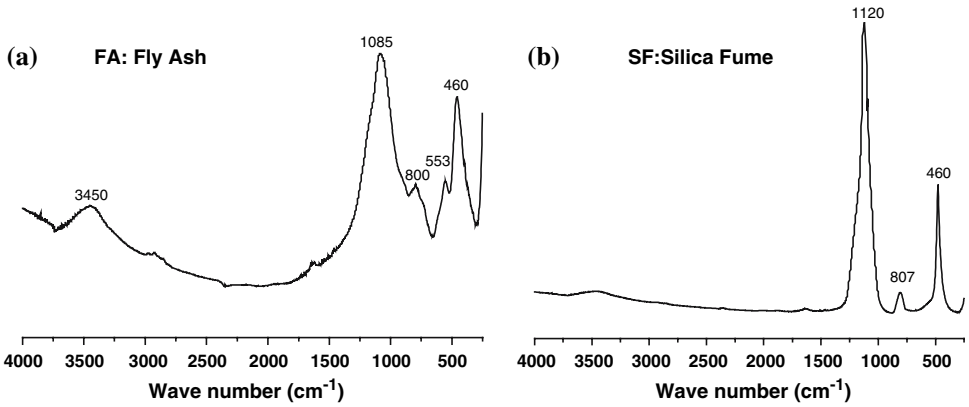

Fig. 1 Mid-IR spectra of fly ash (FA) and silica fume (SF)

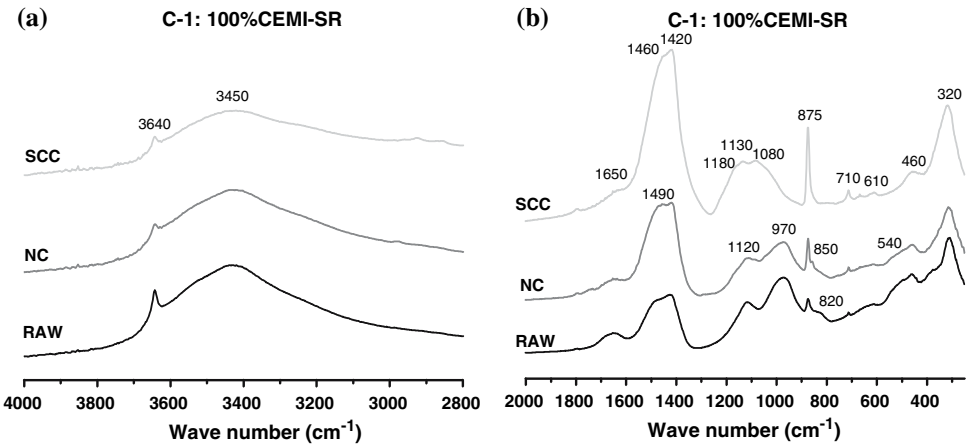

Fig. 2 Mid-IR spectra of raw and treated 100% CEM I-SR cement pastes (C-1). Undried KBr pellets

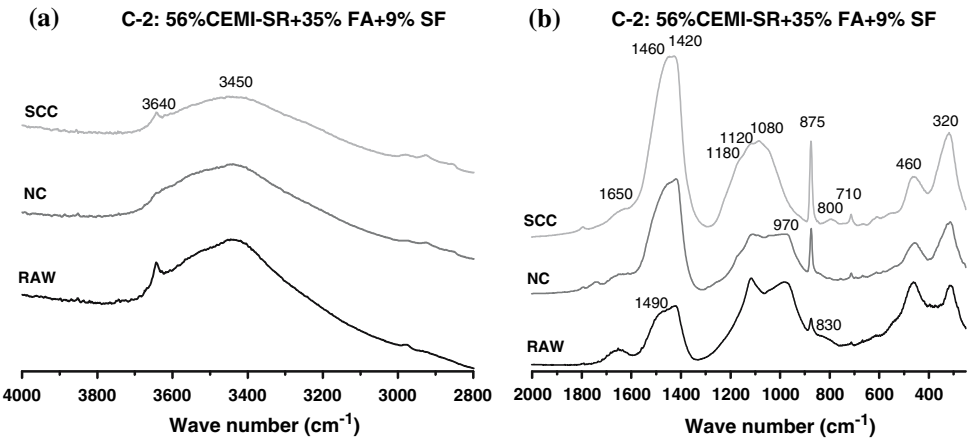

Fig. 3 Mid-IR spectra of raw and treated 56% CEM I-SR + 35% FA + 9% SF cement pastes (C-2). Undried KBr pellets

studies that suggest there is a minimum of three co-existing CSH phases [22]: a tobermorite-like CSH (poly), a dimeric CSH (di-), and a mixed CSH containing both dimer and polymerized (di, poly-) (band at 970 cm^{-1} for dimeric CSH, and overlapped bands centred at 1,040, 1,080, and ~1,130 cm^{-1} attributed to CSH mixes).

More characteristic ettringite bands appear at 1,120 cm^{-1} (SO_4^{2-} asymmetrical stretching), 1,000 cm^{-1} (SO_4^{2-} symmetrical stretching), 820 cm^{-1} (Al–OH bending vibrations in AlO_6), and 540 cm^{-1} (Al–OH bending vibrations in AlO_6) [23]. However, the Si–O stretching bands usually obscure the 1,000 cm^{-1} band and possibly the 1,120 cm^{-1} band. The ettringite bands at 1,120, 820, and 540 cm^{-1} can be distinguished for raw and naturally carbonated C-1 and C-3 samples (Figs. 2a and 4a), having lower intensity in naturally carbonated mixtures, due to the partial decalcification and dissolution of ettringite. In the case of blended sample (C-2), bands at 1,120 cm^{-1} are attributed to silica fume. For supercritically carbonated sample, broad band of silicates overlaps ettringite sulphate bands (1,100 and

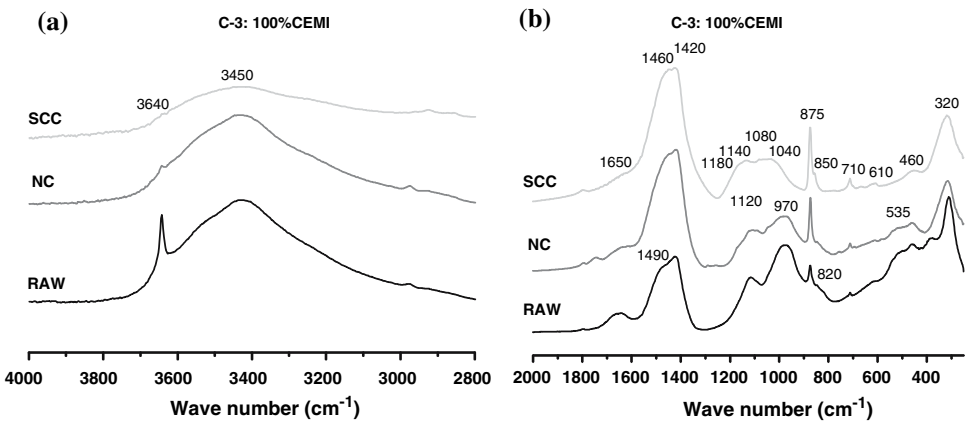

Fig. 4 Mid-IR spectra of raw and treated 100% CEM I cement pastes (C-3). Undried KBr pellets

1,120 cm^{-1}). The dissolution of ettringite can be followed in this case by the disappearance of bands at 820 and 540 cm^{-1}. The intensity decrease of ettringite bands in naturally carbonated samples is interpreted as a partial dissolution of this solid phase due to carbonation process. Bands of ettringite disappear for supercritically carbonated samples, as well in this case due to the preferential carbonation of both CSH gel and ettringite.

Amorphous aluminosilicate phases are likely to cause vibration at around 1,070–1,080 cm^{-1} since a similar band position can be observed for natural and glassy aluminosilicate materials [24]. It is also suggested that the appearance of a shoulder at $\sim$1,200 cm^{-1} occurs also for gels CASH with structure 1.1 nm tobermorite type (Ca/Si < 0.8), because of its occurrence for natural aluminosilicates [25]. Thus, the appearance of a maximum at $\sim$1,080 cm^{-1} in supercritically carbonated sample and the shoulder at $\sim$1,200 cm^{-1} is attributed to CSH chain polymerization (which is accompanied by a decrease in Ca/Si ratio) and replacement of Al by Si producing an Al–tobermorite type structure. [24, 25].

Looking at the FTIR curves of blended Portland cement-based materials, we can conclude that the addition of mineral admixtures such as silica fume and fly ash, to cement pastes, causes a similar reorganization of microstructure; a more polymerized and lower Ca form of CSH gel was formed by the reaction between the pozzolan with CH and the typical high-Ca form of CSH gel main fly ash band due to Si–O and Al–O vibrations, located at 1,080 cm^{-1} [24], cannot be discerned due to interferences in absorption with the other mineral phases.

However, the presence of a band at 800 cm^{-1} in supercritically carbonated cement pastes, which is more noticeable for blended cement paste C-2, is attributed to AlO_4. This fact is an indication that aluminium could substitute silicon when a CSH gel with a low Ca/Si ratio has been formed. The formation of a CASH matrix is related with the decalcification process [26]. To summarize, condensation reactions leading to Si–O–Si bonds occur; however, reactions involving Si–OH and Al–OH groups, i.e. Si–O–Al or aluminosilicate bonds can also occur. High-frequency bands (1,200 cm^{-1}) are clearly related to Si–O–Al mixed vibrations, and the band at 800 cm^{-1} is related with O–Al–O in AlO_4 tetrahedra. These bands have been assigned in accordance with generally accepted practice for the silicate and aluminosilicate families of compounds [27–29].

Because of their different crystal structure the three polymorphs of calcium carbonate (calcite, vaterite, and aragonite) can be discriminated using a vibrational technique, i.e. infrared spectroscopy. Nevertheless the interpretation of appropriate bands is a difficult task since there is a strong overlapping. Additionally it is generally accepted that particle size plays a considerable role on the shape of the infrared spectra. Previous reports have demonstrated the inverse relation between particle size and the intensity of the absorption peaks [30]. In this work, different crystal morphologies and particle sizes of calcium carbonate are expected, depending on the carbonation process. The characteristic bands of calcite can theoretically be found at 1,421, 874, and 713 cm^{-1}. Reference samples show the bands of calcite at 1,420, 875, and 710 cm^{-1} and a band at 1,490 cm^{-1} attributed to vaterite; however, the small band at 850 cm^{-1} and the appearance of a maximum at 1460 cm^{-1} indicate the presence of aragonite. For supercritically carbonated samples the main polymorph is calcite, mixed with aragonite (bands at 850 and 1,460 cm^{-1}).

The band at 320 cm^{-1} is due to Ca–O vibrations in portlandite, CSH gel, and calcium carbonate. The increase in intensity of this band after carbonation is related with the precipitation of $CaCO_3$.

The amount of remaining free water in the samples decreased significantly when carbonating using supercritical conditions. For the naturally treated cement pastes, the amount of free water diminished only slightly with respect to raw cement pastes.

Thermal analysis

Figure 5 presents the differential thermal analysis, DTA, curves for cement pastes. The first endotherm peak, centred around 90 °C, is induced by free or evaporable water. This peak changes with carbonation, and it is transformed into a broad endothermic peak for supercritically carbonated samples, which suggest lower amounts of free water in these treated samples. However the broad temperature range of this endothermic effect for supercritically treated samples (25–200 °C) can be attributed to the loss of two different water types: free water (until 105 °C) and physically adsorbed water of low energy, from CSH or CASH gel.

The loss of free water (~105 °C) has been quantified. TG results showed that the remaining free water after carbonation on the samples was different depending on the processing method. The samples treated under supercritical conditions were highly dehydrated, since the free water at 105 °C was ~2 wt%. This contrasts with the value found for the raw materials that was about 5–7 wt%, and for the naturally carbonated, where the evaporable water was ~4–5 wt% in treated samples.

The slight valley below 400 °C in atmospherically treated samples has been ascribed in the present study to the dehydration of Al–OH and/or Si–OH bonds of CASH matrices. According to the literature [31], the silica hydrogarnet ($C_3AS_{3-x}H_{2x}$ $x = 0$–3) precedes Al-substituted 11 Å tobermorite formation and it has been detected in Portland cement systems due to the dissolution of ettringite.

The endothermic valleys ranging 450–550 °C in DTA curves of carbonated samples are related also with different steps of the dehydration process in aluminosilicates with a structure similar to zeolites. The flattened form of the peaks is related with a high fineness or low crystallinity [32]. The presence of both endotherms at 340 and 530–560 °C, in atmospherically carbonated samples, indicates the presence of CASH matrices.

The endothermic peak at 425–480 °C is due primarily to decomposition of portlandite. The corresponding endotherm for naturally carbonated sample has a lower temperature peak than untreated and supercritically carbonated samples indicating lower amount of portlandite in this sample. In fact, the reacted amount of portlandite calculated from TG curves was considerably larger for samples stored under atmospheric conditions than for the supercritically treated ones (Table 3). The decrease of the decomposition temperature observed for naturally carbonated cement pastes may be also attributed to imperfections of the crystal lattice: a part of OH^- ions was substituted with time by CO_3^{2-} ions, derived from the carbon dioxide contained in air, and this causes an increase in basal spacing of portlandite [33]. Dehydroxylation of $Ca(OH)_2$ was observed for all the samples with the exception of the fully carbonated C-3 sample. In this case the higher alkali content of cement plays an important role in the kinetics of carbonation, accelerating the step in which the CO_2 is combined with OH^- of the pore solution to form CO_3^{2-} which reacts with portlandite to form $CaCO_3$.

The loss of weight between ~600 and 800 °C was assumed to represent the decomposition of $CaCO_3$ which is

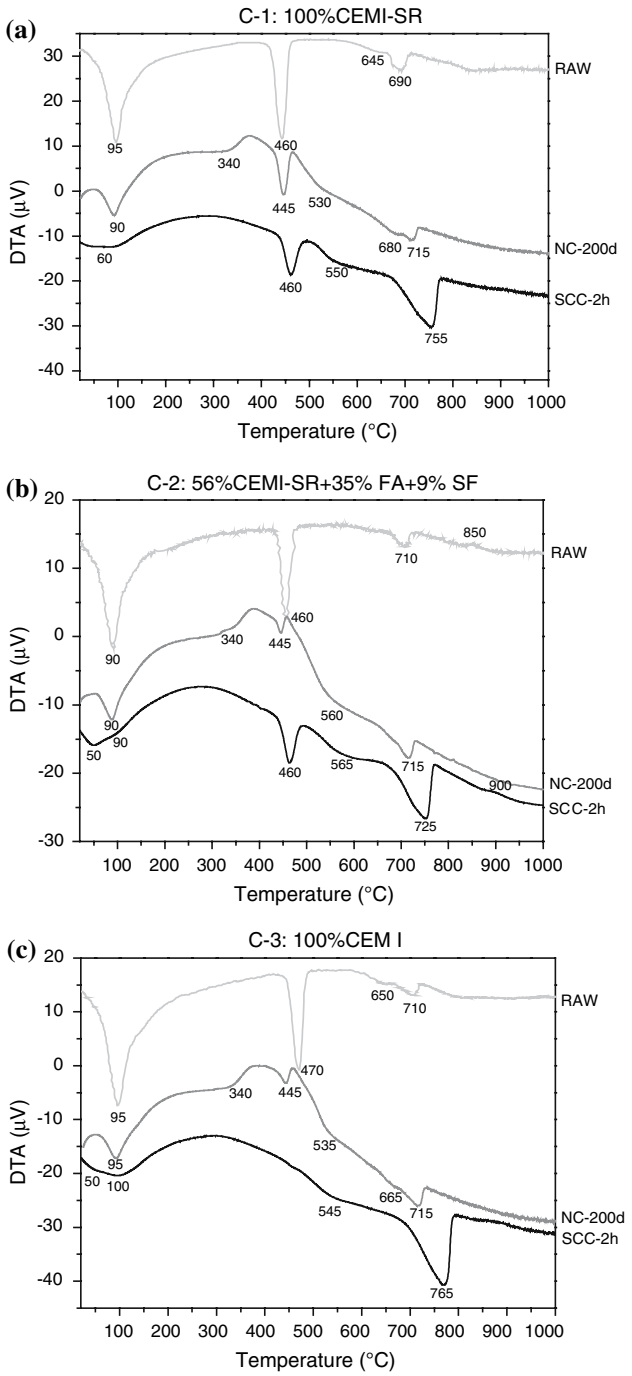

Fig. 5 DTA of cement pastes. Raw, reference materials; NC-200d, 200 days naturally carbonated; SCC-2h, 2 h high CO_2-pressure treated

Table 3 Weight lost (wt%) of water, portlandite, and carbonates for the three samples before any treatment and after natural and supercritical carbonation

Sample	Treatment	Water 105 °C (wt%)	Portlandite			Carbonates		
			T_i	T_f	wt%	T_i	T_f	wt%
C-1	Raw	5.8	410	465	3.1	610	710	4.5
	NC	5.2	425	465	2.0	640	730	6.4
	SCC	2.1	435	490	2.2	570	775	10.7
C-2	Raw	5.3	430	470	2.2	675	720	1.5
	NC	4.1	430	455	0.6	660	730	4.0
	SCC	2.2	440	485	1.4	660	770	8.0
C-3	Raw	6.9	440	490	1.7	610	725	3.0
	NC	4.6	410	460	1.3	645	730	7.1
	SCC	2.1	–	–	–	680	790	11.9

usually a mixture between the three polymorphs (vaterite, aragonite, and calcite). Carbonates show distinctive decomposition peaks at the temperature range of 625–875 °C. In both the raw and the natural carbonated samples, the CO_2 started to be expelled from the carbonate at approximately 680 °C and ended at 730 °C. However, in the $SCCO_2$-treated samples, decarbonation occurred at 680–770 °C. It is suggested that in the $SCCO_2$-treated samples the precipitated calcium carbonate is more crystalline than in the atmospherically carbonated ones, and its amount is higher. Hence, more crystalline samples start undergoing decarbonation at a higher temperature to what would be expected. The two endothermic effects in some samples can be related with the presence of different types of $CaCO_3$ polymorphs or different crystallinity degree.

The amount of calcium carbonate was significantly larger for the $SCCO_2$-treated samples in comparison with naturally treated compounds (Table 3). These results suggested that during the 200-day treatment at atmospheric conditions, the crystallized calcite came mainly from the carbonation of the portlandite phase, since the amounts of $Ca(OH)_2$ reacted and $CaCO_3$ formed were very similar (if both are expressed as CaO). The measured amount of crystallized calcite after supercritical treatment did not correspond to what would be expected if only carbonation of the reacted portlandite took place. Instead, the amount of calcite formed was about fivefold to sixfold higher than that corresponding to full carbonation of reacted portlandite. Therefore, other solid phases containing Ca^{2+}, and not only portlandite, were carbonated and contributed to calcite formation in these cases.

Electron microscopy and microanalysis

Some BSEM micrographs of raw and SC-carbonated cement pastes are presented in Fig. 6. For raw materials, alite and belite grains (less coloured grains) were observed (the EDX spectrum shows the ratio Ca/Si ≈ 3 and 2). Particles of nonreacted FA and SF mineral additions can be also observed in sample C-2. The blended cement paste, sample C-2, was the less compacted paste which is characteristic of mixtures with a large degree of mineral addition and a short hydration time. The Ca/Si ratio in the paste of untreated cement revealed a significant variation from one region to another. The ratio of Ca/Si in uncarbonated C-1 and C-3 samples varied from 1.5 to 2.3, and this is attributed to the difficulty in ionic transport within the paste; thus the metastable equilibrium may be attained only locally on a micrometer range. Compositional variations for C-2 paste ranged from 1.3 to 2.2, indicating that the pozzolanic reaction occurred to some extent.

Carbonated samples are a more dense and featureless groundmass of amorphous material intimately mixed with microcrystalline calcium carbonate with dark inclusions that appear to be remnants of unhydrated cement particles. The Ca/Si ratio could not be measured after carbonation treatment, because Ca content increased sharply as was observed by EDX, due to the precipitation of $CaCO_3$.

Figure 7a highlights the cement–FA interfase after supercritical carbonation. The EDX analysis of areas 1 and 2 indicates that fly ash is partially reacted, and it has formed a CASH matrix as can be observed in spectrum 7a-2. It is reasonable to suggest that the carbonation of CSH containing mineral additions such as fly ash may result in the incorporation of Al (or other constituents) into the polymerizing silicate framework. The supercritical carbonation conditions allow to increase the reaction rate of fly ash.

Figure 7b shows the chemical analysis of sample C-3 and the areas 1 and 2 highlighted in Fig. 6. The difference in grey levels in treated C-3 samples resulted from large differences in the Ca and Si contents, and it means that carbonation led to well-defined reaction zones. The chemical changes as detected by EDX can be observed in Fig. 7b-1 and b-2.

Some more images were selected to be representative as far as the condition of the cement paste and the interface of paste–mineral addition are concerned and are also shown in Fig. 8. In the micrograph shown in Fig. 8a–c, a particle of SF can be observed in detail with $CaCO_3$ crystals grown on its surface.

Finally, Fig. 8d–f shows some micrographs of a macropore filled with $CaCO_3$ crystals. The presence of $CaCO_3$ in the form of calcite or aragonite can be observed because the morphologies of the formed crystals are quite distinct. Calcite has an equilibrium rhombohedral crystal habit (Fig. 8f) [34, 35], and aragonite shows a needle-like morphology (Fig. 8b–c). These morphological differences observed in $CaCO_3$ formed in an air void or those

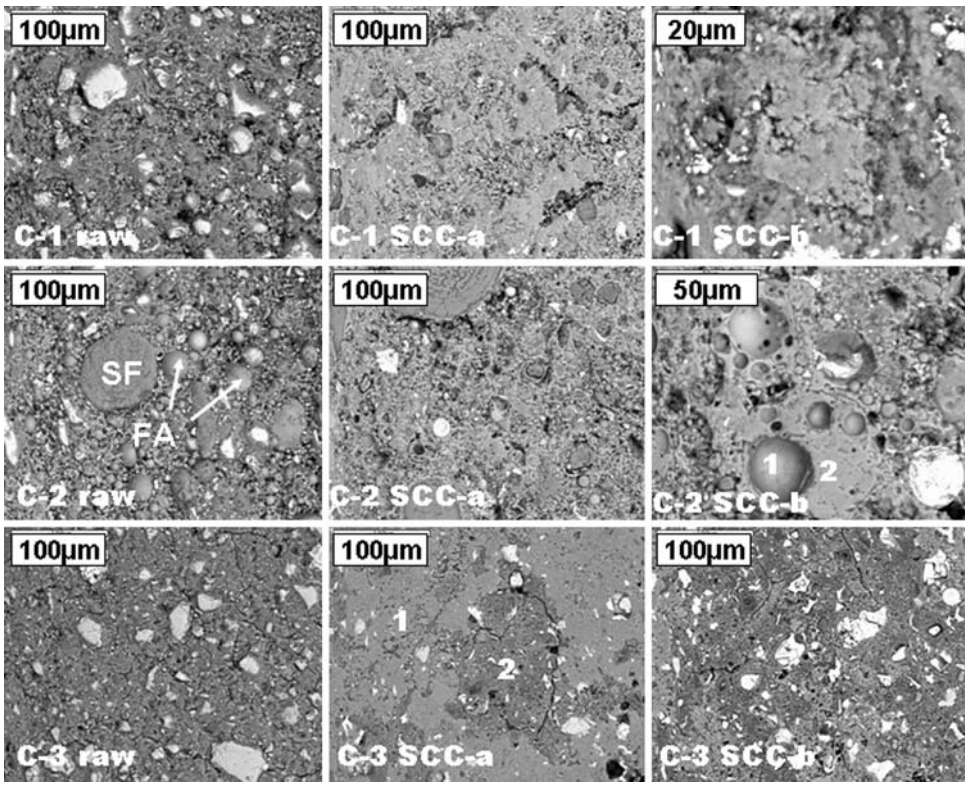

Fig. 6 BSEM micrographs of the raw and treated cement pastes

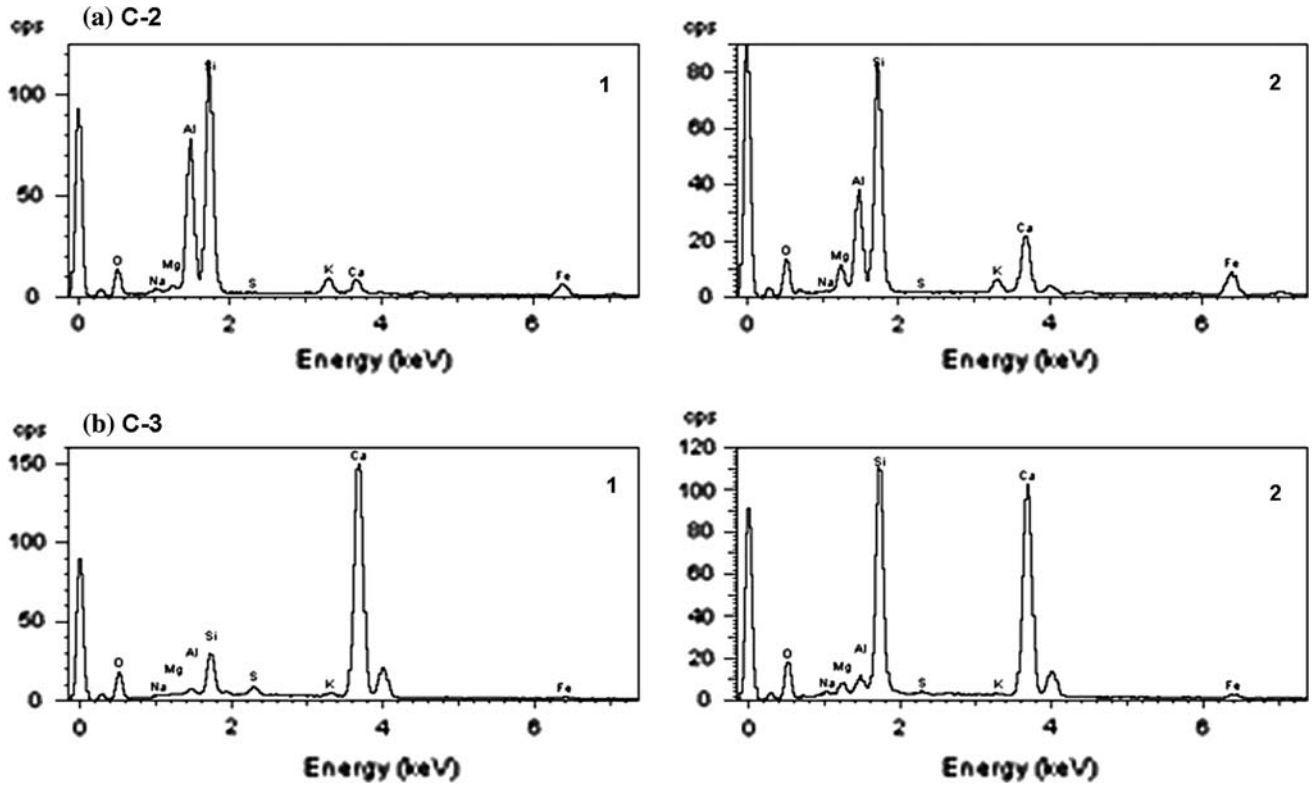

Fig. 7 EDX microanalysis of areas 1 and 2 in C-2 and C-3, highlighted in Fig. 6

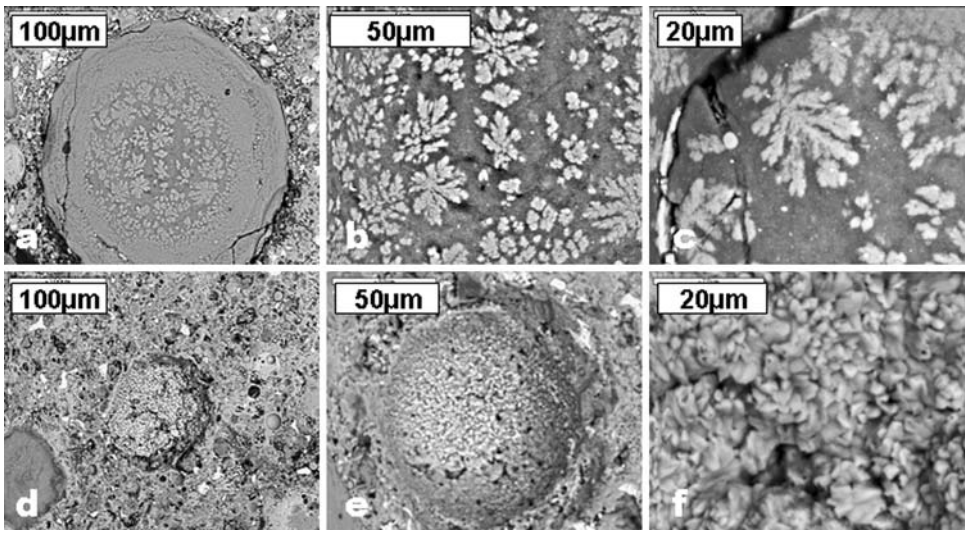

Fig. 8 BSEM micrographs of C-2 paste: $CaCO_3$ crystals in SF grain (**a–c**) and $CaCO_3$ crystals in an air void (**d–f**)

crystallized on a SF grain, can be found in inhomogeneities in chemical composition of the surrounding pore solution.

Interpretation

The supercritical treatment alters the bulk chemical and structural properties of cement pastes by accelerating carbonation reactions (from months to hours), while at the same time reducing free water. Carbonation has influenced the properties of cement pastes in a number of ways.

Effect of binder type

The alkali of cement favours the concentration of OH^- in the pore solution for counteracting the positive ionic charge of K and Na. In this sense, the alkali in cement favours its carbonation. Then, the explanation for the total dissolution of portlandite in C-3 sample (based on the cement with the higher alkali content, CEM I) can be found by the reaction:

$$CO_2 + 2OH^- \rightarrow CO_3^{2-} + H_2O$$

The CO_2 first dissolves in the pore solution and then reacts with the OH^-, forming CO_3^{2-}. This reaction depends on the concentration of OH^- and CO_2 in the pore solution; in other words, on the alkali content of cement.

In the supercritical treatment of C-1 and C-2 pastes, results suggested that carbonation of portlandite was not completed and was substituted by the carbonation of CSH and ettringite. Interpretation is that deposits of crystalline $CaCO_3$ were formed on the surface of the $Ca(OH)_2$ particles, inhibiting further dissolution of this phase.

Carbonation involves reaction with phases like AFt/AFm (ettringite and monosulphate), CSH gel, and CH. CSH gel products are significantly altered. The gel becomes progressively polymerized as OH and Ca are consumed in the production of $CaCO_3$. Intensified carbonation of pastes based in Portland cements produces a geopolymeric structure. CSH or CASH structures consist of a polymeric Si–O–Si or Si–O–Al framework, similar to that found in natural aluminosilicates. Accurate identification and proof of coexistence of phases such as Al–tobermorite and Si–hydrogarnet are a priority for analysts due to their relation with the durability of building products [36].

The process can be summarized as:

- Partial dissolution of portlandite.
- Dissolution of ettringite.
- Decalcification of CSH gel.
- Silicate polymerization.
- Possible incorporation of tetrahedral and/or hexagonal aluminium in polymerized gel resulting in the formation of an aluminosilicate gel.
- Compensation of charge due to the silicon substitution for aluminium could be made by alkalis from the pore solution. The substitution of $2Al^{3+}$ for $(Si^{4+} + Ca^{2+})$, i.e., the incorporation of both tetrahedral and octahedral aluminium, should also be considered.

Influence of carbonation method for Portland cement-based materials

The pattern with regard to depletion of $Ca(OH)_2$ and formation of $CaCO_3$ observed during FTIR analysis was confirmed by thermal analysis. Both analysis techniques indicated that samples treated under supercritical conditions during 2 h were carbonated to a larger extent than those naturally carbonated for 200 days. Differences were due to the distinctive way of CO_2 addition to the system.

In the natural carbonation treatment, samples were stored in an open vessel exposed to atmosphere. In these conditions, the amount of CO_2 dissolved in the pore water, and

hence available CO_3^{2-} for carbonation, is restricted by the low solubility of atmospheric CO_2 in water (0.06 mol%) [20, 37, 38]. The atmospheric process led to the accumulation of an excess of $Ca^{2+}_{(aq)}$ in the growth medium.

At the studied high pressures, the ease of absorption, penetration, and diffusion of large amounts of $SCCO_2$ into the micropores of the cement provides continuous availability of fresh reactant [14, 18].

$CaCO_3$ polymorphs

In CO_2-treated samples, either natural or intensified, calcite was the main carbonate polymorph formed, although aragonite and vaterite were found, as shown in the FTIR spectra corresponding to natural and supercritical carbonation. The precipitation of the stable calcite polymorph as the main phase is the habitual result for carbonation processes where solid $Ca(OH)_2$ is suspended in the media and heterogeneous nucleation induced by foreign particles is favoured. Some authors pointed out that calcite is formed from carbonation of $Ca(OH)_2$ and CSH gel, and aragonite is formed when the Ca/Si ratio in the CSH gel was low [20]. This result could indicate a preferential $SCCO_2$ carbonation of CSH gel leading to aragonite formation in the final stages when the Ca/Si ratio in CSH was low, or in the transition zone paste-silica fume grains, where the Ca/Si ratio is also low.

Conclusions

The carbonation reaction using compressed CO_2 could be used for the production of a broad range of carbonated cement-based materials; the process led to an accelerated carbonation in comparison with natural carbonation (from months to hours). The comparison of the results obtained by DTA/TGA, FTIR, and BSEM/EDX, of the raw and carbonated cement pastes, led to the conclusions presented below.

Total dissolution of portlandite in pastes based on CEM I (high alkali and C_3A content) is explained by the presence of alkalis in cement favouring its carbonation. The type of binder and the addition of mineral admixtures such as silica fume and fly ash, to cement pastes, causes a similar reorganization of microstructure; a more polymerized and lower Ca form of CSH gel formed in this case by decalcification of high-Ca form of CSH gel. The increase of polymerization and order in the sequence of TO_4 (T = Si or Al) tetrahedron packing, can be followed by a splitting of the main FTIR silicate band, into several components and the presence of a band at 800 cm^{-1}. It is well known that decalcified CSH gels increase the durability of concrete.

The overall results indicate that the naturally carbonated pastes differ somewhat in microstructural characteristics from that of the supercritically carbonated samples. Results suggested that during the treatment at atmospheric conditions, the crystallized calcium carbonate came mainly from the carbonation of the portlandite phase. The lower portlandite content was confirmed by FTIR and thermal analysis. Less polymerization of the CSH gel was confirmed by the lower FTIR silicate band frequencies. In the supercritical treatment, results suggested that deposits of crystalline $CaCO_3$ formed on the surface of the $Ca(OH)_2$ particles inhibit further dissolution of this phase.

All the three $CaCO_3$ polymorphs were formed in carbonated pastes, i.e. calcite, aragonite, and vaterite. The presence of $CaCO_3$ in the form of calcite, vaterite, or aragonite was detected by FTIR; additionally calcite and aragonite were identified by BSEM because of the different morphologies. Calcite was the main polymorph in carbonated pastes; however, aragonite presence is also important and its formation is related with the presence of a CSH with a low Ca/Si content produced by decalcification of the primary CSH or by the CSH formed in the surroundings of a silica fume grain.

Acknowledgements The financial support of Comunidad de Madrid Project GR/AMB/0451/2004, Région Poitou-Charentes (Convention 06/RPC-R-84) and EU Project STRP SurfaceT NMP2-CT-2005-013524 is greatly acknowledged. Carlos A. García-González acknowledges CSIC for its funding support through a I3P fellowship.

References

1. Senevirtane AMG, Short NR, Page CL (2003) Compos: Part A 34:1105
2. Short NR, Bough AR, Seneviratne AMG, Purnell P, Page CL (2004) J Mater Sci 39:5683. doi:10.1023/B:JMSC.0000040076.42260.cb
3. Macias A, Kindness A, Glasser FP (1997) Cem Concr Res 27(2):215
4. Alba N, Vázquez E, Gassó S, Baldasano JM (2001) Waste Manage 21:313
5. Garrabrants AC, Sánchez F, Kosson DS (2004) Waste Manage 24:19
6. Hartmann T, Paviet-Hartmann P, Rubin JB, Fitzsimmons MR, Sickafus KE (1999) Waste Manage 19:355
7. Van Ginneken L, Dutré V, Adriansens W, Weyten H (2004) J Supercrit Fluids 30:175
8. Fernández Bertos M, Simons SJR, Hills CD, Carey PJ (2004) J Hazard Mater B112:193
9. Al-Kadhimi TKH, Banfill PFG, Millard SG, Bungey JH (1996) Adv Cem Res 8(30):47
10. Soroushian P, Aouadi F, Chowdhury H, Nossoni A, Sarwar G (2004) Cem Concr Compos 26:797
11. Bary B, Sellier A (2004) Cem Concr Res 34:1859
12. Jones Jr (1996) US patent 005518540A
13. Van Gerven T, Van Baelen D, Dutre V, Vandecasteele C (2004) Cem Concr Res 34:149
14. Short NR, Purnell P, Page CL (2001). J Mater Sci 36:35. doi:10.1023/A:1004870204162

15. Ngala VT, Page CL (1997) Cem Concr Res 27(7):995
16. Johannesson B, Utgenannt P (2001) Cem Concr Res 31:925
17. Arandigoyen M, Bicer-Simsir B, Alvarez JI, Lange DA (2006) Appl Surf Sci 252:7562
18. García-González CA, Hidalgo A, Andrade C, Alonso MC, Fraile J, López-Periago AM, Domingo C (2006) Ind Eng Chem Res 45:4985
19. García-González CA, Hidalgo A, Fraile J, López-Periago AM, Andrade C, Domingo C (2007) Ind Eng Chem Res 46:2488
20. Goñi S, Gaztañaga MT, Guerrero A (2002) J Mater Res 17(7):1834
21. Xu P, Kirckpatrick RJ, Poe B, McMillan PF, Cong X (1999) J Am Ceram Soc 82(3):742
22. Grutzeck MW (1999) Mater Res Innov 3:160
23. Farcas F, Touzé Ph (2001) Bull lab Ponts Chaussées 230:77
24. Lee WKW, van Deventer JSJ (2002) Colloids Surf A: Physicochem Eng Asp 211:49
25. Farmer VC (ed) (1974) The infrared spectra of minerals. Mineralogical Society, London
26. Hidalgo A, Petit S, Domingo C, Alonso C, Andrade C (2007) Cem Concr Res 37:63
27. Sitarz M, Mozgawa W, Handke M (1999) J Mol Struct 511–512:281
28. Mozgawa W (2001) J Mol Struct 596:129
29. Mozgawa W, Sitarz M (2002) J Mol Struct 614:273
30. Vagenas NV, Gatsouli A, Kontoyannis CG (2003) Talanta 59:831
31. Klimesch DS, Ray A (1999) J Therm Anal Calorim 56:27
32. Kalousek GL (1957) J Am Ceram Soc 40(3):74
33. Stepkowska ET (2006) J Therm Anal Calorim 84(1):175
34. Tai CY, Chen W-R, Shih S-M (2006) AIChE J 52(4):292
35. O'Connor WK, Dahlin DC, Rush GE, Dahlin CL, Collins WK (2002) Miner Metall Proc 19(2):95
36. Ray A (2002) Pure Appl Chem 74(11):2131
37. Daimon M (1971) J Am Ceram Soc 54:423
38. Groves GW, Rodway DI, Richardson IG (1990) Adv Cem Res 3(11):117